Influence of Zhengzhou Metro Shield Construction on Adjacent Structures and Strata: A Case Study of an Existing Subway Station

Zhengya ZHANG [1], Changshun HAO [2], Yong YAN [3], Jinwei FU [2], Hadi HAERI [4], Vahab SARFARAZI [5] *

[1] *College of Engineering, Zhengzhou Technology and Business University, Zhengzhou 451400, China*
[2] *School of Civil Engineering and Transportation, North China University of Water Resources and Electric Power, Zhengzhou, 450046, China*
[3] *Henan Water Conservancy Investment Group, ZhengZhou 450002, China*
[4] *Department of Mining Engineering, Higher Education Complex of Zarand, Shahid Bahonar University of Kerman, Kerman, Postal Code:7761146934, Kerman, Iran*
[5] *Department of Mining Engineering, Hamedan University of Technology, Postal Code:65155-579, Hamedan, Iran*

http://doi.org/10.5755/j02.ms.41086

Received 7 April 2025; accepted 6 May 2025

This paper analyzes the Zhengzhou Metro Line, focusing on a case with an existing structure in its alignment. It uses shield construction methods and on-site survey data, employing Midas GTS NX software for finite element analysis. A numerical model for an underpass beneath a subway station was created through displacement back analysis to identify optimal layer thickness. The study examined deformation and stress in the surrounding strata and the station during the construction of a double-line shield. Findings revealed that the station's stiffness and end pre-treatment significantly limited strata displacement, with maximum settlement measured at 12.97 mm and uplift at 12.02 mm in the non-underpass section. This research offers valuable insights for metro projects globally, enhancing understanding of shield tunneling impacts on adjacent structures.
Keywords: deformation, stress, Midas GTS NX software, displacement back analysis method.

1. INTRODUCTION

Shield tunneling has been used extensively in China for nearly five decades and is now the primary method for constructing most domestic subways. It has significantly contributed to urban rail transit, highway construction, and urban drainage system renovations [1 – 5]. Furthermore, settlement may happen as a result of earthquakes occurring during or after the construction process [6 – 8]. Li et al. [9] shared findings from an in-situ monitoring program on displacement and bolt load during the excavation of a powerhouse cavern in China, underscoring the need for precise deformation monitoring to improve support systems. Strokova [10] developed a numerical model for surface subsidence from subway tunneling in Munich, validating it with field data and identifying key factors. In follow-up work, Strokova [11] proposed methods for estimating surface settlement in urban tunnel construction using both empirical and numerical techniques. Zhang et al. [12] analyzed surface settlement from shield tunneling in soft ground using a 3D finite element method, achieving strong alignment between predictions and actual responses. Houhou et al. [13] studied shallow tunnel excavation deformation in Toulouse using 3D numerical modeling, focusing on fluid-soil interaction and validating results with in situ measurements. Liu et al. [14] studied the Pile-Beam-Arch method for subway construction, highlighting its effectiveness in urban areas. Zhu [15] analyzed shield tunneling's effect on surface settlement and suggested adjusted parameters to reduce ground movement near sensitive structures. Fei et al. [16] found that construction joints in tunnels can weaken the surrounding ground's shielding effect, necessitating the reinforcement of double-line shield tunnels with steel pipe piles to prevent settlement while maintaining acceptable tunnel lining stress. Cao et al. [17] tackled challenges of urban subway tunnels near structures, specifically the Jing-Zhang high-speed rail tunnel in Beijing, using the TIA method to manage deformation and reduce surface subsidence. Ding et al. [18] developed a method for underpinning pile foundations of shield tunnels intersecting pile groups, emphasizing controlled settlements and monitoring vault settlements and segment bending moments during excavation. Bao and Wei [19] examined how shallow buried soft rock tunnel excavation affects highway stability, highlighting the importance of managing deformation in V-class tunnels to prevent surface cracking. Wang et al. [20] addressed ground settlement due to urban rail shield tunneling, enhancing prediction accuracy with a data preprocessing technique and a PSO-optimized Back Propagation Neural Network, achieving a maximum relative error of 0.46 %. In Tianjin, Lei et al. [21] found that curvature tunneling led to more soil settlement than straight tunneling, with their predictions closely matching monitoring data. Additionally, Wang et al. [22] developed a buoyancy prediction model for shield tunneling using ISSA-XGBoost-GRU-SVM, significantly reducing root mean square errors compared to traditional

* Corresponding author: V. Safranazi
E-mail: *sarfarazi@hut.ac.ir*

methods. Wang et al. [23] analyzed tunneling-induced pile vibrations in hard rock using a DEM-FDM model, finding that low-frequency vibrations affect nearby piles. Qiang et al. [24] conducted 3D finite element simulations on shallow buried bifurcated tunnels, noting that excavation impacted rock deformation and settlement but remained within safety limits. Wang et al. [25] developed a buoyancy prediction model for shield tunneling using ISSA-XGBoost-GRU-SVM, enhancing predictions by considering excavation and grouting factors, with feature selection through principal component analysis and hyperparameter optimization via a sparrow algorithm. Wang et al. [26] examined subway tunnel excavation's effects on pile vibrations, primarily around 50 Hz, and provided construction guidelines. Qiang et al. [27] studied the safety of shallow buried tunnels and anchorages through 3D simulations, observing significant but acceptable impacts on surrounding rock and building settlement. This paper presents a three-dimensional numerical simulation of a subway station beneath a tunnel. Using the displacement back-analysis method, it determined the equivalent layer thickness that aligns with monitoring conditions. The study measured vertical displacements of the subway station and surrounding strata during tunnel shield construction.

2. ESTABLISHMENT OF UNDERPASS MODEL

2.1. Basic assumptions of numerical calculation

The numerical analysis of the underpass is based on the following assumptions:

1. The soil strata are assumed to be uniformly distributed in a horizontal manner, utilizing the modified Mohr-Coulomb constitutive model.
2. The physical and mechanical properties of the existing subway station are assumed to remain unchanged during the construction of the new tunnel, and their effects are not taken into consideration.
3. Any impacts from other exceptional circumstances are also excluded from this analysis.

2.2. Structural parameters and mesh division

The model consists of six layers of soil, a new shield tunnel, the existing subway station along with its internal supporting structure, an existing subway tunnel, a receiving shaft, and a new station. The properties of the strata and supporting structure are detailed in Table 1 and Table 2.

Table 1. Parameters of mechanical properties of support structures

Structure	Material	Elastic modulus, MPa	Poisson's ratio	Bulk density, kN/m^3
Segments	Reduction of C50	2.45E4	0.2	25
Reinforced segments	C50	3.5E4	0.2	25
Columns	C40	3.25E4	0.2	25
Beams, slabs, ground-connected walls	C35	3.15E4	0.2	25
Grouting layer, freezing reinforcement	/	100	0.2	22.5
Shield	Q235	2.08E5	0.2	78.5

The model dimensions are X×Y×Z = 132 m × 175 m × 50 m, as illustrated in Fig. 1. The negative direction of the X-axis is designated as the tunnel excavation direction. Key specifications include: the diameter of the excavation area is 6.26 m; the burial depth of the tunnel is 25.76 m; the thickness of the segment support structure is 0.35 m, with each ring measuring 1.5 m in length, amounting to a total of 60 rings; the minimum angle between the longitudinal direction of the existing subway station and the excavation direction of the shield tunnel is 75°; there is a minimum vertical clearance of 1.46 m between the new shield tunnel and the existing Line 1 Huanghe South Road Station.

The new shield tunnel runs beneath the subway station and links to the receiving shaft of Line 12 Huanghe South Road Station. The model consists of 489,100 grid units and 249,902 nodes, as shown in Fig. 1.

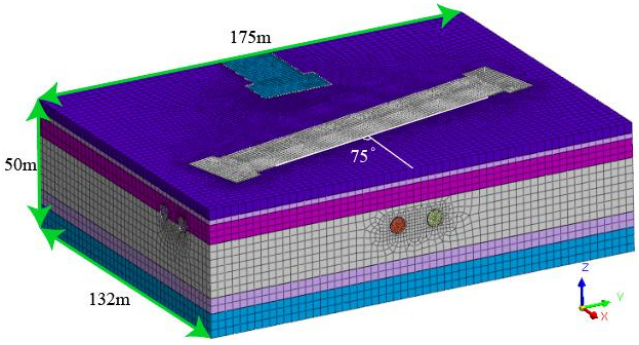

Fig. 1. Schematic mesh of the underpass construction model

Table 2. Parameters of stratigraphic mechanical properties

Soil layer	Thickness, m	Gravity, kN/m^3	Cohesion, KPa	Internal friction angle, °	E_{50}^{ref}, MPa	E_{oed}^{ref}, MPa	E_{ur}^{ref}, MPa	Stress-related power index
Miscellaneous fill soil	4.1	17.5	15	18	8.75	7.875	30.625	0.5
Clayey silt	2	19.5	28	18	8.23	7.407	32.92	0.6
Silty clay	7.5	19.7	30	22	6.75	6.075	27	0.6
Fine sand	21	22.5	0.3	30	21.5	21.5	64.5	0.5
Clayey silt	6	19.4	36	22.3	10.45	9.405	52.25	0.6
Silty clay	9.4	20.1	38	26	9.95	8.955	49.75	0.6

Fig. 2 shows the main structures of the finite element model, including the new Line 12 subway station and its structures (A), the existing Line 1 subway station (B), the existing Line 1 shield tunnel (D), and the new Line 12 shield tunnel (E). The special treatment is the horizontal freezing reinforcement treatment at the receiving end (C).

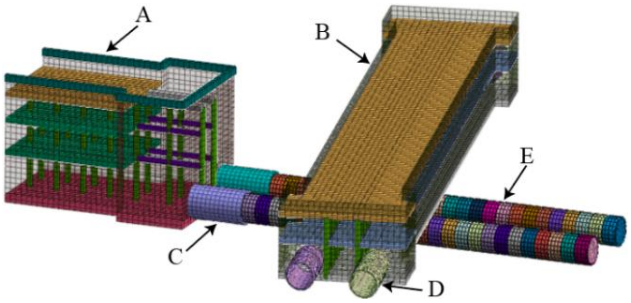

Fig. 2. Major structures: A – new Line 12 subway station; B – existing Line 1 subway station; C – horizontal freezing reinforcement treatment; D – existing Line 1 shield tunnel; E – new Line 12 shield tunnel

The newly built Line 12 and existing Line 1 at Huanghe South Road Station comprise key components, including crown beam, top plate, bottom plate, middle plate, longitudinal beams, ground-connected wall, and columns. The backfill soil on the top plate of Line 12 has not yet been added. Structural components will be modeled as units in GTS NX, while other structures will use solid units. Fig. 3 shows the newly constructed shield tunnel for Line 12, highlighting the original soil mass, pipe segment, grouting layer, and a 60 mm thick shield shell. The extraction function in GTS NX will create the shell unit to simulate the shield machine's outer shell.

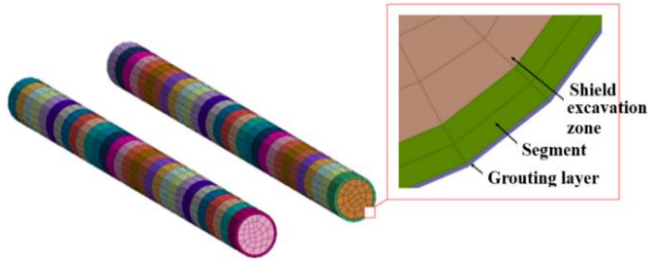

Fig. 3. Schematic diagram of the grid division of the shield tunnel of the new Line 12

The segment unit is depicted in Fig. 4. It has an inner diameter of 5.5 meters and a thickness of 0.35 meters. The length of a single ring is 1.5 meters. The excavation length for both the left and right lines of the model is set at 90 meters.

The shield machine features a front shield measuring approximately 6 meters. This front shield is necessary for the segment assembly. To accurately simulate the length of the unlined segment section, simplifications of the construction phase steps are proposed. This approach aims to reduce the time required for numerical simulation calculations of the shield model.

The simulation covers various processes, including shield excavation, segment assembly, grouting, and lining. For these simulations, a cycle advance of 3 meters is utilized. This length corresponds to the length of two rings of segments.

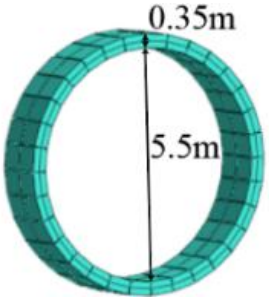

Fig. 4. Schematic diagram of concrete lining grid division

During the segment splicing process, the bolt connection between the blocks and rings is considered. A reduction in segment stiffness is achieved by multiplying the segment's elastic modulus by 0.7. No strength reduction is applied during the underpass stage, as the selected segment is reinforced.

3. DISPLACEMENT BACK ANALYSIS - EQUAL LAYER CALIBRATION

The synchronous grouting simulation method for the shield tail in this model utilizes shell elements. The "equal layer" is considered an elastic-plastic body, emphasizing that the grouting layer is treated as homogeneous within the finite element analysis framework. A Poisson's ratio of 0.2 is applied, as it has a minimal impact on stratum deformation. In GTS NX finite element software, the material properties of the equal layer can be adjusted at different construction stages. This adjustment simulates the synchronous grouting of the shield tail gap. The elastic modulus after hardening is set at 100 MPa.

The thickness of the grouting layer is generally determined by the diameter of the shield machine and the segment. Soil properties also play a significant role in making this determination. An empirical formula is followed for this purpose.

$$\delta = \eta\Delta, \tag{1}$$

where δ is the thickness of equal layers in finite element models; η denotes the grouting layer thickness coefficient; Δ signifies the thickness of the annular gap at the shield tail.

Keiichi [17] analyzed over 150 results to determine the thickness coefficient of the grouting layer across various soil types. For dense sand, the coefficient ranges from 0.9 to 1.8, making it suitable for this model since the excavation is in dense sand. The shield machine cutter head diameter is 6,260 mm, and the segment's outer diameter is 6,200 mm. The equivalent layer thickness is calculated based on the four conditions in Table 3 for comparison with monitoring data.

Table 3. Thickness space functions of equal generation layers

Working conditions	Thickness function		Coordinate system
Condition 1	$d = -(2/313)$	$h + 0.06$	Overall
Condition 2	$d = -(2/313)$	$h + 0.08$	Overall
Condition 3	$d = -(2/313)$	$h + 0.10$	Overall
Condition 4	$d = -(2/313)$	$h + 0.12$	Overall

The displacement back analysis method compared actual measured values from eight locations on the ground during left-line shield tunneling with numerical simulations at various equivalent layer thicknesses. As illustrated in Fig. 5, Condition 3 closely matched the surface settlement values obtained from actual measurements. Therefore, this non-uniform thickness function was selected for numerical calculations throughout the entire construction process and reinforcement conditions.

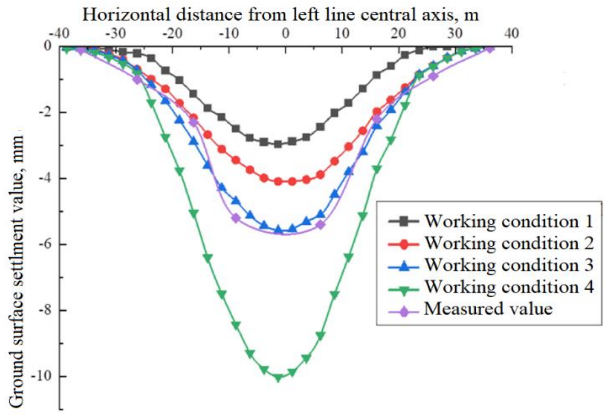

Fig. 5. Surface vertical displacements and measured values under different thicknesses of isoparaffin layers

4. CONSTRUCTION LOAD PARAMETERS

4.1. Soil compartment pressure

The soil pressure within the soil compartment is measured by a sensor. This pressure is controlled by adjusting several factors: the thrust of the propulsion cylinder, the propulsion speed, the screw conveyor speed, and the opening of the slag gate. The calculation for the soil pressure at the excavation surface is outlined below.

$$P_1 = \sum_{i=1}^{i=n} K_{0i}\gamma_i H_i, \tag{2}$$

where P_1, K_{0i},, γ_i, and H_i represent the static earth pressure on the excavation face; the lateral pressure coefficient of the soil layer; the severity of layer 1 soil; and the thickness of the first soil layer, respectively.

The calculation of excavation surface water pressure is as follows:

$$P_2 = \sum_{i=1}^{i=n} \gamma_i H_i, \tag{3}$$

where P_2, γ_i, and H_i is the static water pressure at the excavation face, the severity of soil in Layer 1, and the thickness of the first soil layer, respectively.

When the support pressure from the soil compartment on the excavation face exceeds the combined pressures of water and soil, the ground surface will rise. On the other hand, if the support pressure is less than this combined pressure, the surface will settle.

The ideal condition for earth pressure balance during shield excavation is to maintain the soil compartment support pressure equal to the total water and soil pressures at the excavation face while the excavation progresses. Due to the design of the cutterhead, the pressure on the excavation face is not uniform. Instead, it gradually increases in a linear manner from the top of the cutterhead to the bottom.

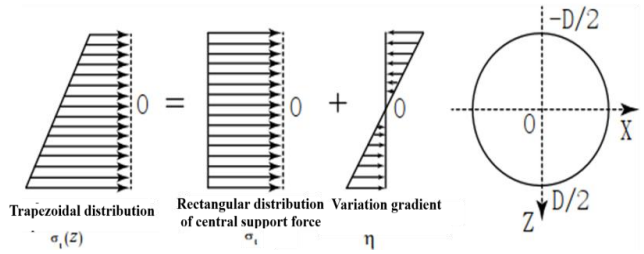

Fig. 6. Trapezoidal support pressure distribution in the tunnel; illustrates how increased shield diameter leads to higher soil pressure and greater support force differences

As illustrated in Fig. 6, the soil pressure within the tunnel diameter will rise as the shield diameter increases. This increase results in a corresponding rise in the difference in support forces.

Typically, the support force at the excavation face exhibits a trapezoidal distribution. As shown in Fig. 7, the spatial distribution function of the face pressure is calculated based on construction experience, with a variable representing the depth of the space.

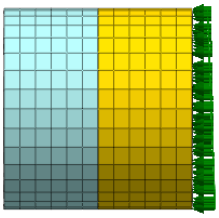

Fig. 7. Pressure distribution in the soil compartment of the Shield, depicting variations in pressure levels across different zones

4.2. Segment thrust value

The segment thrust is a critical load in earth pressure balance shield excavation. The maximum thrust of the shield machine used in this project can reach 35100 kN. Based on empirical values from similar projects, the observed thrust range in the stratum is between 18000 kN and 25000 kN.

To minimize damage to the segment while effectively completing the construction, the thrust for this numerical simulation has been set at 20000 kN. In the model, a thrust of 6 bar is applied to the segment. This pressure is uniformly distributed and acts on the segment in the opposite direction of the excavation. This setup is illustrated in Fig. 8.

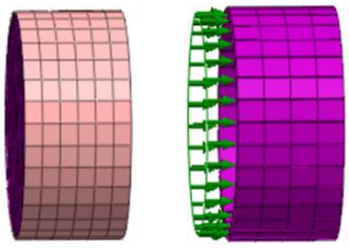

Fig. 8. Distribution of thrust force on tube sheet, illustrating the thrust applied in the opposite direction of the excavation and its uniform pressure distribution across the segment

4.3. Grouting pressure value

Choosing the correct grouting pressure is crucial for minimizing disturbances to the soil during shield excavation. If the grouting pressure is too high, it can cause fatigue damage to the connecting bolts between the segments. This may lead to misalignment, which could result in engineering accidents.

On the other hand, if the grouting pressure is too low, the grouting liquid may not fully occupy the gap at the shield tail. This could lead to inadequate support for the soil and potentially cause bottom settlement.

In the simulation, the grouting pressure was set to 0.25 MPa. This pressure was oriented along the normal direction of the outer contour of the segment, as illustrated in Fig. 9.

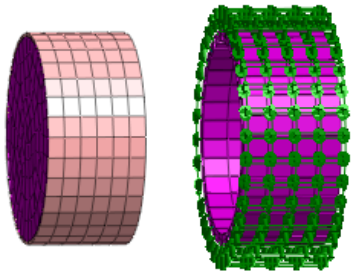

Fig. 9. Grouting pressure distribution at the shield tail, illustrating the pressure oriented along the normal direction of the outer contour of the segment

5. NUMERICAL CALCULATION PROCESS OF UNDERPASS

In Fig. 10, a step-by-step calculation of the underpass simulation is presented.

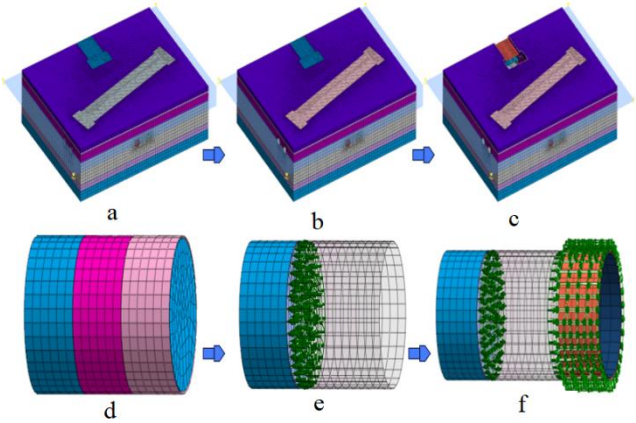

Fig. 10. Step-by-step calculation of underpass simulation

– Establishing the initial stress field:
a) the stress stage type is set. The stratum activated, self-weight and boundary conditions for model displacement inputted. The overall underground static water level defined at –12.1 m. Displacement zeroing performed.
– Construction of existing subway stations and tunnels:
b) the stress stage type set. The soil within the existing subway station deactivated. Structural components of the station, including beams, slabs, and columns, activated. Backfill properties on the top plate enabled. Properties of existing tunnel units adjusted.
– Construction of new subway stations:
c) the stress stage type set. Soil in the excavation area of the new subway station's foundation pit deactivated. Structural components of the new station, such as beams, slabs, columns, and ground walls, activated. Displacement zeroing performed.
– Left line tunnel excavation (S1):
d) the stress stage type set. Original soil in the first step excavation area deactivated. Support pressure of the first step excavation soil chamber and corresponding shield properties activated.
– Left line tunneling (S2):
e) the stress stage type set. Original soil within the second step excavation area deactivated. Support pressure and shield shell properties from the first step deactivated. Support pressure for the second step excavation soil chamber and shield tail grouting pressure activated. Assembly of segments completed. Thrust applied to segments during this excavation step activated. Shield tail grouting layer properties enabled. Grouting pressure for this stage deactivated.
– Left line excavation to the reinforcement area:

When excavation reaches S26, soil properties of the horizontal freezing reinforcement area activated as the end well approached by the left line. Unit properties modified until the left line tunnel excavation process completed.
– Right line excavation:

Upon reaching step S29 in the left line excavation, excavation for the right line commenced. The same procedure followed as that of the left line until both lines completed.a) Set the stress stage type. Activate the stratum and input the self-weight and boundary conditions for model displacement. Define the overall underground static water level at –12.1 m. Perform displacement zeroing.
– Construction of existing subway stations and tunnels:
b) set the stress stage type. Deactivate the soil within the existing subway station. Activate the structural components of the station, including beams, slabs, and columns. Enable the backfill properties on the top plate. Adjust the properties of the existing tunnel units.
– Construction of new subway station:
c) set the stress stage type. Deactivate the soil in the excavation area of the new subway station's foundation pit. Activate the structural components of the new station, such as beams, slabs, columns, and ground walls. Perform displacement zeroing.
– Left line tunnel excavation (S1):
d) set the stress stage type. Deactivate the original soil in the first step excavation area. Activate the support pressure of the first step excavation soil chamber along with the corresponding shield properties.
– Left line tunneling (S2):
e) set the stress stage type. Deactivate the original soil within the second step excavation area. Also deactivate the support pressure and shield shell properties from the first step. Activate the support pressure for the second step excavation soil chamber and the shield tail grouting pressure. Complete the assembly of segments. Activate the thrust applied to the segments during this excavation step. Enable the shield tail grouting layer properties. Passivate the grouting pressure for this stage.
– Left line excavation to the reinforcement area:

f) when excavation reaches S26, activate the soil properties of the horizontal freezing reinforcement area as the end well is approached by the left line. Modify the unit properties until the left line tunnel excavation process is complete.

– Right line excavation:

f) upon reaching step S29 in the left line excavation, commence excavation for the right line. Follow the same procedure as that of the left line until both lines are completed.

5.1. Analysis of the influence of strata and existing station structures

It is assumed that the existing subway station and line have established a new equilibrium stress field with the surrounding strata. This stress field serves as the initial state. When constructing the subway using a shield, the original "station-soil" stress field will be disrupted. This disruption leads to a redistribution of stresses in the area.

The existing subway station and the line within the soil have considerable structural stiffness and a large surface area. As a result, they can effectively hinder the propagation of disturbances. This helps to limit soil displacement.

Fig. 11 shows the cumulative vertical displacements of the left line center profile at different excavation stages. During the construction of a shield tunnel beneath a subway station or within an existing large-section underground project, maintaining elastic contact between the tunnel and existing infrastructure can be challenging. This difficulty arises because the station and existing line have a much higher resistance to deformation compared to the surrounding soil.

When construction takes place outside the station area, the station maintains elastic contact with the surrounding soil. This condition allows for coordinated force and displacement interactions. However, once excavation reaches the station area, it can lead to compression and shear failure of the surrounding soil.

If excavation takes place outside the influence zone of the existing structure, the displacement tends to be significant. This is influenced by the presence of plastic zones in the rock and soil. Conversely, when the shield tunnel is excavated within the influence range of the station's structural stiffness, the station and existing line can resist deformation more effectively.

As a result, this situation yields lower displacement compared to the surrounding soil, which may create voids.

Surface settlement caused by a new shield tunnel passing through an existing station should be less than in sections where it does not. For instance, the maximum surface settlement during the left line's excavation occurs from the beginning of the excavation to the influence zone of the station, peaking at 5.79 mm. However, during the phase from the start of the underpass to the completion of excavation, the maximum surface settlement at the top of the existing station is just 1.13 mm.

This difference in settlement occurs primarily due to the higher resistance to deformation in the station's support structure, in contrast to the unpassed area of the soil.

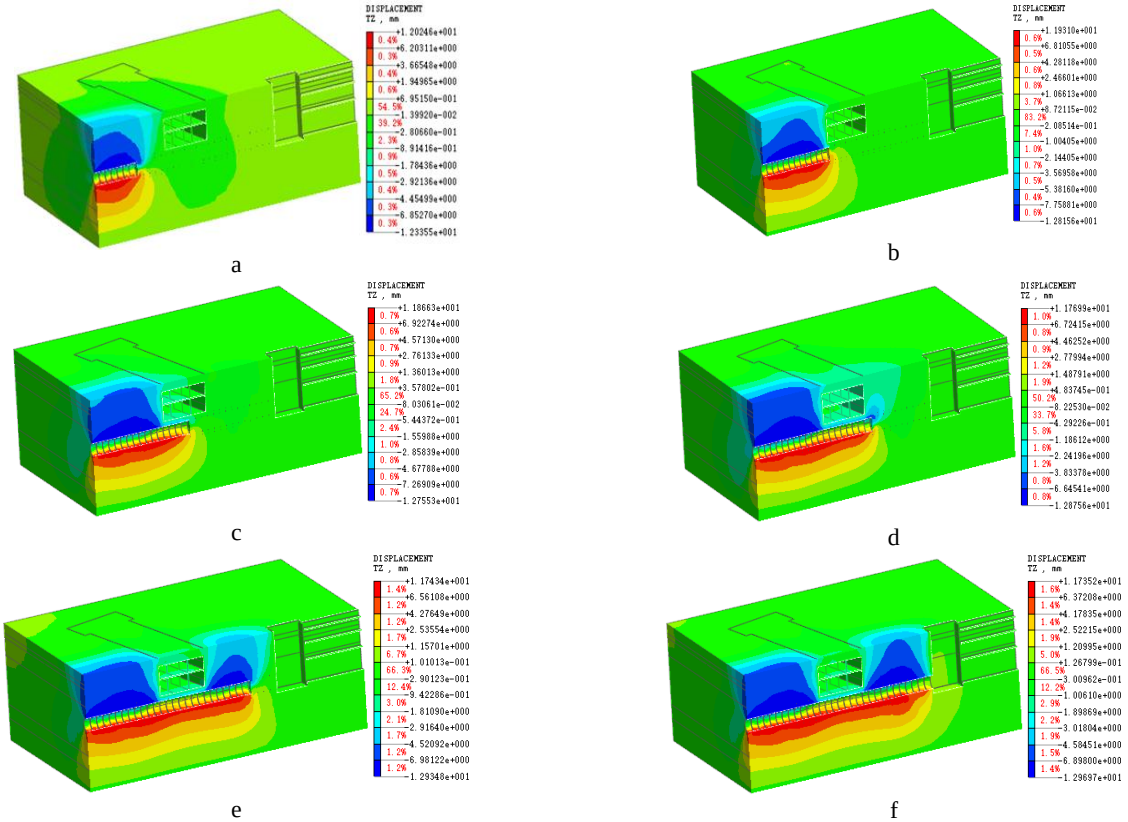

Fig. 11. Cumulative vertical displacements of the left line profile during excavation: a – excavation to the station front; b – downward crossing begins; c – descent to intersection center; d – downward penetration completed; e – excavation to reinforcement area; f – excavation completed.

This resistance reduces the extent of surface disturbance caused by construction activities. Additionally, the vertical stress exerted by the existing station on the soil below is significantly lower than that of the original soil.

During the excavation of the left line, the maximum uplift of the soil beneath the arch bottom is recorded at 12.02 mm in areas that have not yet been traversed. In contrast, during the underpass stage, the maximum uplift recorded at the arch bottom is 8.61 mm. The vertical displacement of the soil beneath the arch bottom in a specific range is less than that experienced during the unpassed stage.

In the horizontal freezing reinforcement area at the front end of the left line, vertical displacement of the stratum is effectively minimized. When the left line shield passes under the station to the reinforcement area, the maximum settlement at the tunnel crown measures 10.57 mm. The maximum uplift at the arch bottom during this stage is 10.16 mm. Within the reinforcement area, the maximum settlement at the arch crown reaches 7.94 mm, while the maximum uplift at the arch bottom is 6.29 mm.

Fig. 12 illustrates the cumulative vertical displacements of the right line center profile at different excavation stages. The displacement evolution of the vertical section model during the excavation of the right line is illustrated in Fig. 12. Overall, its trend is comparable to that of the left line excavation. However, there is a notable difference related to the underpass area.

During the right line excavation, the maximum surface settlement occurred within the influence range of the existing station. This settlement was observed from the beginning of the excavation until its completion. The maximum surface settlement at the top plate of the existing station's covering soil was only 1.16 mm. Throughout the right line excavation, the maximum uplift beneath the arch bottom reached 11.57 mm. This maximum uplift occurred in soil areas that were not directly beneath the station.

During the underpass stage, the maximum uplift at the arch bottom was recorded at 8.53 mm. In the small area between the right line shield tunnel and the reinforced section beneath the station, the maximum settlement at the tunnel crown was measured at 10.13 mm. The maximum uplift under the arch bottom in this area was 9.95 mm. In the soil reinforcement area at the tunnel's end, the maximum settlement at the arch crown was 7.61 mm, while the maximum uplift at the arch bottom was 6.30 mm. As illustrated in Fig. 13, when the shield tunnel passes close to the existing subway station, it can cause disturbances to the main structure.

However, due to the overall structural rigidity of the station, no significant deformation occurred during the construction process.

After completing the construction of the left tunnel line, the maximum settlement deformation of the station's main structure was measured at 1.99 mm. The right line recorded a maximum deformation of 1.85 mm. Both measurements were taken at the edge of the ground wall and the station floor. This highlights the need to analyze the stress deformation characteristics of the station floor.

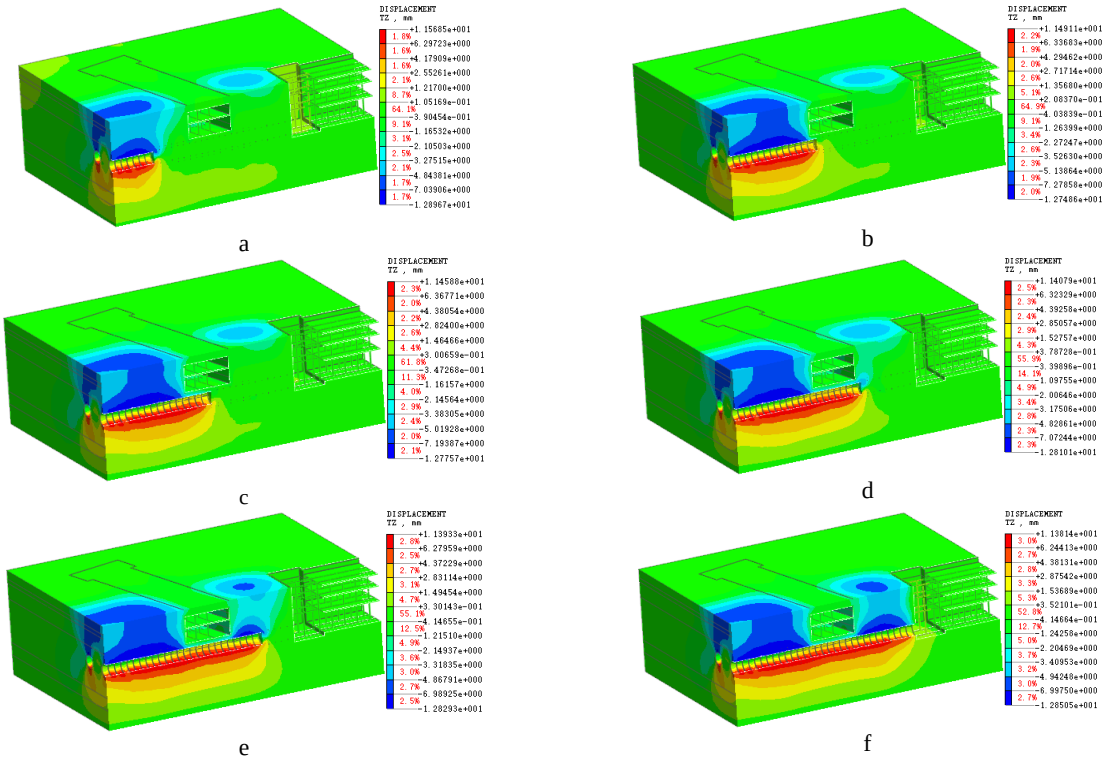

Fig. 12. Cumulative vertical displacements of the right line center profile at different excavation stages: a – excavation to the station front; b – downward crossing begins; c – line descends to intersection center; d – downward penetration completed; e – excavation to front reinforcement; f – right line excavation finished

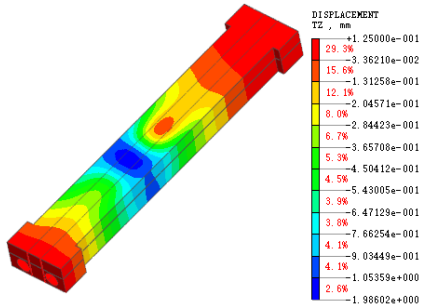

a

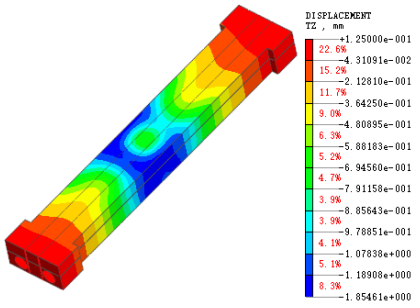

b

Fig. 13. Cumulative vertical displacement observed at the entire station: a – completion of left line excavation; b – completion of right line excavation

5.2. Analysis of stress deformation characteristics of the station floor and longitudinal beams

When the shield tunnel runs close to the subway station, it can impact the main structure of the station. One critical area affected is the excavation unloading zone, which is nearest to the station floor. This can influence the existing roadbed and track.

Two main factors contribute to these impacts:

1. During excavation, the shield machine disrupts the surrounding soil. This can lead to soil deformation. The interaction between the soil and the station floor may result in issues such as sinking, cracking, or breaking of the floor. These problems affect the structural stability and durability of the station.
2. The bottom longitudinal beam may be affected by the additional thrust from the shield machine. There are also factors like the gap between the shield tail and the frictional shear of the shield shell. These changes can alter the internal forces acting on the beam and affect its bearing capacity.

As shown in Fig. 14, when the shield passes underneath the floor slab near the station, the pressure in the soil compartment is slightly less than the effective stress at that site. This difference leads to some settlement in the station floor slab. Before the left line goes through the subway station, the maximum vertical settlement of the floor slab reaches 0.542 mm. This maximum occurs directly beneath the centerline of the left line tunnel. On both sides of the floor slab, the maximum uplift observed is 0.163 mm in the longitudinal direction.

As excavation for the left line continues and reaches the halfway point, the maximum vertical settlement of the floor slab increases to 2.065 mm. However, the uplift on both sides of the slab remains stable. Once the left line has completely passed through and excavation is finished, the maximum vertical settlement stabilizes at about 1.99 mm.

When the right line begins to pass, the maximum vertical settlement deformation of the floor slab decreases from 1.95 mm to around 1.85 mm before stabilizing.

The deformation and stress of the bottom longitudinal beam at each stage are shown in Table 4. The maximum vertical displacement of the bottom longitudinal beam is 1.95 mm. This value is nearly the same as that of the bottom plate.

When the right tunnel is underpassed, the maximum horizontal displacement reaches 0.59 mm. In comparison to the scenario without the underpass, the maximum bending moment of the bottom longitudinal beam increases by 578 kN·m. This increase could potentially lead to slight cracks.

In general, when the distance between two tunnels is short, the first tunnel excavated creates a prestressing effect on the second tunnel. Moreover, the reverse bending effect of the bottom longitudinal beam helps to mitigate the impact of the later-excavated tunnel on the station's bottom plate. As a result, the displacement and stress trends of the bottom longitudinal beam during the construction of the right tunnel remain relatively stable.

6. CONCLUSIONS

This paper presents a case study of a subway running through a building in China, analyzed using Midas GTS NX software and the finite element method. The key conclusions are as follows:

1. The displacement back analysis method determines the optimal thickness function of the grouting isotope layer, expressed as $d = -(2/313)h + 0.1$.
2. During dual-line asynchronous tunneling, factors like station stiffness and soil stress release significantly impact soil displacement. The maximum settlement and uplift measured in the excavation area were 5.65 mm and 8.61 mm, respectively.

Table 4. Bottom longitudinal beam deformation and force at each stage

Stage	Maximum vertical displacement, mm	Maximum horizontal displacement, mm	Maximum bending moment, kN·m
Before the left line passes under the bottom	0.15	0.12	1828.2
The left line passes under the middle of the bottom plate	1.55	0.04	2034.1
The left line passes under the bottom plate	1.93	0.45	2391.7
Before the right line passes under the bottom plate	1.95	0.46	2394.6
The right line passes under the bottom plate	1.92	0.46	2405.9
The right line passes under the bottom plate	1.85	0.59	2393.7

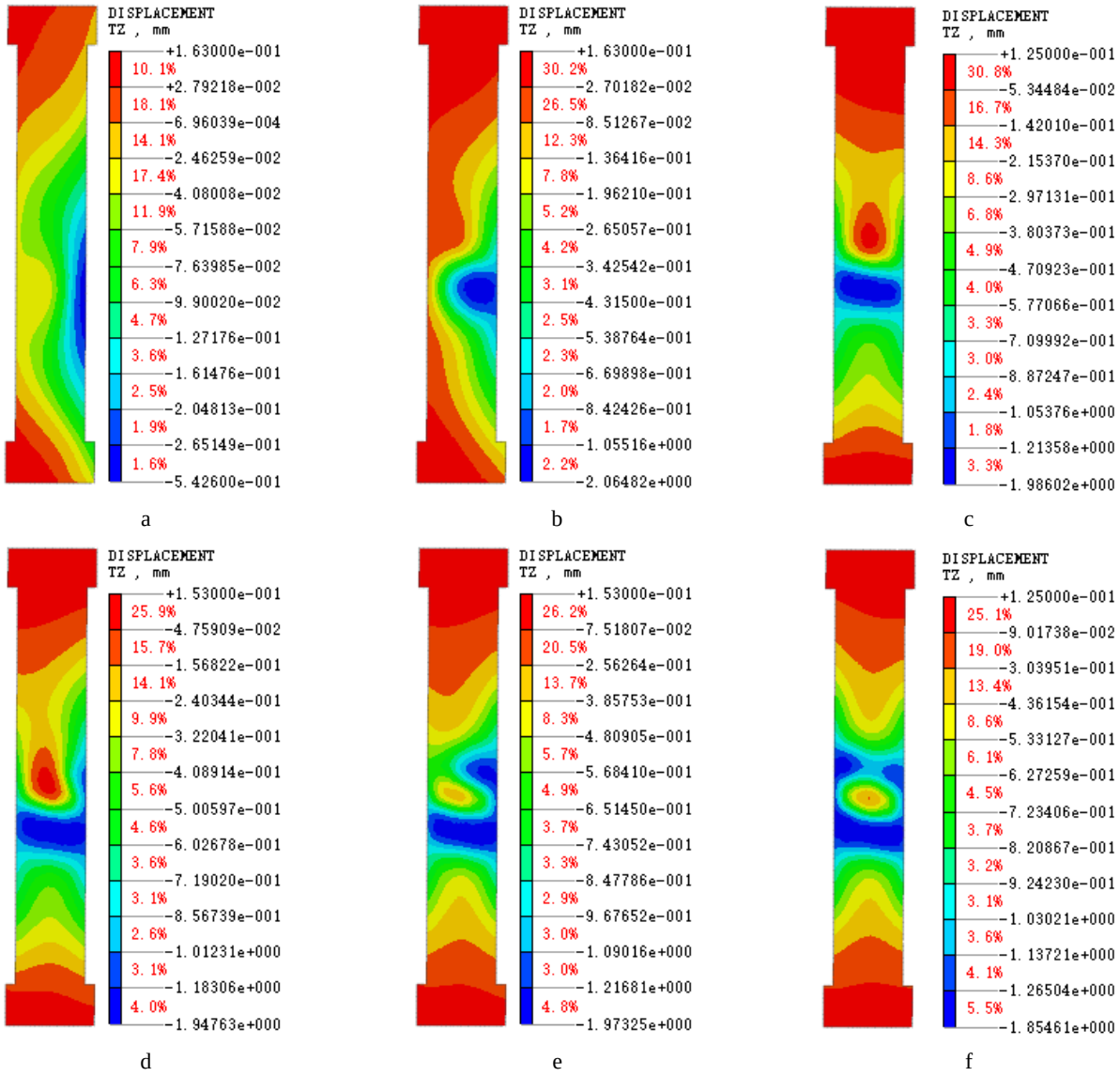

Fig. 14. Vertical displacement of the station floor during the construction of the double-lane asynchronous shield structure: a – before left line passage; b – left line under the floor; c – left line excavation complete; d – before right line passage; e – right line under the floor; f – right line excavation complete

3. After excavating both left and right lines, the station's maximum settlement was 1.99 mm and 1.84 mm, with negligible uplift. The left line's passage through the floor slab center resulted in a maximum cumulative displacement of 2.06 mm.
4. Before the right line passed, the maximum settlement of the bottom longitudinal beam was 1.95 mm. After its passage, the maximum horizontal displacement was 0.59 mm. When the right line crossed the floor slab's center, the maximum bending moment on the bottom longitudinal beam was 2405.9 kN·m.
5. These results greatly influence subway tunnel design and construction in cities, optimizing plans, improving monitoring, and enhancing safety and stability for sustainable urban rail systems.

Acknowledgments

This work was supported by National Natural Science Foundation of China (No. 52479100), National Foreign Experts Program of China (No. S20240157 and No. H20240271), and Outstanding Foreign Scientist Studio of Henan Province (No. GZS2025015).

REFERENCES

1. **Zhang, Z., Huang, M.** Geotechnical Influence on Existing Subway Tunnels Induced by Multiline Tunneling in Shanghai Soft Soil *Computers and Geotechnics* 56 2014: pp. 121 – 132. https://doi.org/10.1016/j.compgeo.2013.11.008
2. **Wang, Z., Zhang, K.W., Wei, G., Li, B., Li, Q., Yao, W.J.** Field Measurement Analysis of the Influence of Double Shield Tunnel Construction on Reinforced Bridge

Tunnelling and Underground Space Technology 81 2018: pp. 252 – 264.
https://doi.org/10.1016/j.tust.2018.06.018

3. **Xu, Q., Lei, S., Zhu, Y., Zhao, W., Wang, C., Wang, D.** Theoretical Prediction Model for Surface Settlement Caused by the Excavation of New Tunnels Undercrossing Existing Tunnels Based on Modified Stochastic Medium Theory *KSCE Journal of Civil Engineering* 26 2022:pp. 4136 – 4145.
https://doi.org/10.1007/s12205-022-1911-6
4. **Shi, C.H., Cao, C.Y., Lei, M.F.** An Analysis of the Ground Deformation Caused by Shield Tunnel Construction Combining an Elastic Half-Space Model and Stochastic Medium Theory *KSCE Journal of Civil Engineering* 21 (5) 2017:pp. 1933 – 1944.
https://doi.org/10.1007/s12205-016-0804-y
5. **Ding, Z., Tu, W., Li, X.** Enhancing Ground Loss Rate Prediction in Soft-Soil Shield Tunneling: A Synergistic Approach of Peck Back Analysis and eXtreme Gradient Boosting and Bayesian Optimization *Scientific Reports* 14 2024: pp. 21935.
https://doi.org/10.1038/s41598-024-73025-3
6. **Shats'kyi, I.P., Struk, A.B.** Stressed State of Pipeline in Zones of Soil Local Fracture *Strength Materials* 41 2009: pp. 548 – 553.
https://doi.org/10.1007/s11223-009-9165-9
7. **Bulat, A.F., Dyrda, V.I., Grebenyuk, S.N., Agal'tsov, G.N.** Methods for Evaluating the Characteristics of the Stress-Strain State of Seismic Blocks Under Operating Conditions *Strength of Materials* 51 2019: pp. 715 – 720.
https://doi.org/10.1007/s11223-019-00129-x
8. **Wan, Z., Cao, W., Jiang, P.H., Liu, Y.Y.** Analytical Solution of Cylindrical Cavity Expansion in the Construction Process of Pipe Pile *Strength Materials* 55 2023: pp.426 – 440.
https://doi.org/10.1007/s11223-023-00536-1
9. **Li, S., Yu, H., Liu, Y., Wu, F.** Results from In-Situ Monitoring of Displacement, Bolt Load, and Disturbed Zone of a Powerhouse Cavern During Excavation Process *International Journal of Rock Mechanics and Mining Sciences* 45 (8) 2008: pp. 1519 – 1525.
https://doi.org/10.1016/j.ijrmms.2008.01.012
10. **Strokova, L.A.** Numerical Model of Surface Subsidence During Subway Tunneling *Soil Mechanics and Foundation Engineering* 46 2009: pp. 117 – 119.
https://doi.org/10.1007/s11204-009-9050-3
11. **Strokova, L.A.** Methods of Estimating Surface Settlement During Driving of Urban Tunnels *Soil Mechanics and Foundation Engineering* 47 2010: pp. 92 – 95.
https://doi.org/10.1007/s11204-010-9094-4
12. **Zhang, Z.X., Shen, M.J., Teng, L.** Back-Analysis of the Response of Shield Tunneling by 3D Finite Element Method *Journal of Shanghai Jiaotong University (Science)* 18 2013: pp. 298 – 305.
https://doi.org/10.1007/s12204-013-1398-x
13. **Houhou, M.N., Emeriault, F., Vanoudheusden, É.** Three-Dimensional Back-Analysis of an Instrumented Shallow Tunnel Excavated by a Conventional Method *Geotechnical and Geological Engineering* 34 2016: pp. 1101 – 1117.
https://doi.org/10.1007/s10706-016-0031-9
14. **Liu, X., Liu, Y., Yang, Z., He, C.** Numerical Analysis on the Mechanical Performance of Supporting Structures and Ground Settlement Characteristics in the Construction Process of Subway Station Built by Pile-Beam-Arch Method *KSCE Journal of Civil Engineering* 21 2017: pp. 1690 – 1705.
https://doi.org/10.1007/s12205-016-0004-9
15. **Zhu, C.** Control of Surface Settlement by Considering Shield Tunneling Technology *KSCE Journal of Civil Engineering* 21 2017: pp. 2896 – 2907.
https://doi.org/10.1007/s12205-017-0761-0
16. **Fei, R., Peng, L., Zhang, C., Zhang, J., Zhang, P.** Experimental and Numerical Studies of a Shield Twin Tunnel Undercrossing the Existing High-Speed Railway Tunnel *Geotechnical and Geological Engineering* 42 2024: pp. 1871 – 1886.
https://doi.org/10.1007/s10706-023-02650-y
17. **Cao, R., Peng, L., Zhao, Y.** Construction Optimization for Subway Interval Tunnels Crossing a High-Speed Rail Shield Tunnel at a Short Distance *Soil Mechanics and Foundation Engineering* 61 2024: pp.177 – 183.
https://doi.org/10.1007/s11204-024-09960-0
18. **Ding, W., Cao, K., Wen, Y., Du, Y., Shang, C., Li, Z., Huang, X.** Analysis of the Influence of Pile Underpinning of the Pile Group Under the Viaduct of the Overlapping Shield Tunnel on the Surrounding Environment *International Journal of Civil Engineering* 22 2024: pp. 1807 – 1833.
https://doi.org/10.1007/s40999-024-00988-9
19. **Bao, L., Wei, F.** Tunnel Construction in Shallow Soft Rock Using the Pipe Shed Support *Scientific Reports* 14 2024: pp. 3401.
https://doi.org/10.1038/s41598-024-53634-8
20. **Wang, Q., Shen, C., Tang, C., Guo, Z., Wu, F., Yang, W.** Machine Learning-Based Forecasting of Ground Surface Settlement Induced by Metro Shield Tunneling Construction *Scientific Reports* 14 2024: pp. 31795.
https://doi.org/10.1038/s41598-024-82837-2
21. **Lei, H., Shi, L., Hu, Y., Zheng, G., Zhang, T., Jia, R.** Ground Movement and Settlement Prediction Induced by Double-Track Curvature Shield Tunneling *Acta Geotechnica* 19 2024: pp. 6179 – 6193.
https://doi.org/10.1007/s11440-023-02144-4
22. **Wang, X., Zhang, J., Song, W., Guo, F., Yao, C.A.** Segment Flotation Prediction Model for Shield Tunnel Construction Based on a Hybrid Neural Network *Geotechnical and Geological Engineering* 42 2024: pp. 5539 – 5556.
https://doi.org/10.1007/s10706-024-02845-x
23. **Wang, Y., Ma, Y., Wang, R., Ding, B., Yu, S.** Vibration Response of Piles at Different Distances Induced by Shield Tunneling in Hard Rock Strata *Scientific Reports* 14 2024: pp. 21723.
https://doi.org/10.1038/s41598-024-72987-8
24. **Qiang, L., Fengmin, C., Yangyong, C., Hanlin, L., Xiaoguang, J.** Analysis of Influence of Anchor Excavation of Shallow Buried Bifurcated Tunnel and Adjacent Tunnel on Overlying Buildings. In: Liu, T., Liu, E. (eds) Proceedings of the 2nd International Conference on Advanced Civil Engineering and Smart Structures. ACESS 2023 . Lecture Notes in Civil Engineering, vol 474. Springer, Singapore, 2023.
https://doi.org/10.1007/978-981-97-1514-5_52
25. **Wang, X., Wang, M., Jiang, R., Xu, J., Li, B., Wang, X., Yu, J., Su, P., Liu, C., Yang, Q., Lei, M., Liao, X.** Structural Deformation Monitoring During Tunnel Construction: A Review *Journal of Civil Structural Health Monitoring* 14 2024: pp. 591 – 613.
https://doi.org/10.1007/s13349-023-00741-1

26. **Wang, Y., Ma, Y., Wang, R., Ding, B., Yu, S.** Vibration Response of Piles at Different Distances Induced by Shield Tunneling in Hard Rock Strata *Scientific Reports* 14 2024: pp. 21723. https://doi.org/10.1038/s41598-024-72987-8

27. **Keiichi, F.** Shield Tunneling Method: Ground Settlement and Loosening from the Perspective of Foundation Engineering *Tunnel Translations Series* 5 1985: pp. 49 – 63 (in Chinese).